



Titre: Rheological behavior of cellulose nanocrystal suspensions in polyethylene glycol
Title:

Auteurs: Quentin Beuguel, Jason Robert Tavares, Pierre Carreau, & Marie-Claude Heuzey
Authors:

Date: 2018

Type: Article de revue / Article

Référence: Beuguel, Q., Tavares, J. R., Carreau, P., & Heuzey, M.-C. (2018). Rheological behavior of cellulose nanocrystal suspensions in polyethylene glycol. Journal of Rheology, 62(2), 607-618. <https://doi.org/10.1122/1.5010789>
Citation:

 **Document en libre accès dans PolyPublie**
Open Access document in PolyPublie

URL de PolyPublie: <https://publications.polymtl.ca/3005/>
PolyPublie URL:

Version: Version finale avant publication / Accepted version
Révisé par les pairs / Refereed

Conditions d'utilisation: Tous droits réservés / All rights reserved
Terms of Use:

 **Document publié chez l'éditeur officiel**
Document issued by the official publisher

Titre de la revue: Journal of Rheology (vol. 62, no. 2)
Journal Title:

Maison d'édition: Society of Rheology/AIP
Publisher:

URL officiel: <https://doi.org/10.1122/1.5010789>
Official URL:

Mention légale: ©2018. This is the author's version of an article that appeared in Journal of Rheology (vol. 62, no. 2) . The final published version is available at <https://doi.org/10.1122/1.5010789>
Legal notice:

Rheological behavior of cellulose nanocrystal suspensions in polyethylene glycol

Quentin BEUGUEL, Jason R. TAVARES, Pierre J. CARREAU, Marie-Claude HEUZEY

Department of Chemical Engineering, CREPEC – Research Center on High Performance Polymer and Composite Systems, Polytechnique Montreal, Montreal, QC, H3T 1J4, Canada.

Corresponding author: Marie-Claude Heuzey (E-mail: marie-claude.heuzey@polymtl.ca), +1 (514) 340-4711 ext. 5930

Abstract

The rheological behavior of cellulose nanocrystals (CNCs) in polar media based on polyethylene glycol (PEG) was investigated from aqueous suspensions to nanocomposites. The aim of this work is to improve our knowledge on the CNC behavior in polymer media and develop rheological indices to characterize the dispersion of nanoparticles in polymer matrices. CNCs were obtained from sulfuric acid hydrolysis of wood pulp and supplied after a spray- or freeze-drying process. Ultrasonication was used to break agglomerates and disperse CNCs in aqueous suspensions before mixing with an aqueous PEG solution at room temperature. The samples were subsequently dried and compression molded. From capillary and oscillatory shear rheology, no adsorption of PEG chains on CNCs could be detected, as many had previously hypothesized. The increase of PEG concentration in aqueous suspension favored the gelation by depletion effect and suggested CNC orientation. Viscoelastic properties and transmission electronic images of PEG/CNC nanocomposites highlighted the formation of a percolated network of CNCs for low concentrations ≥ 0.15 vol%. From Shih *et al.*'s model, a fractal dimension of 2 was obtained for these percolated nanocomposites, suggesting a 2D network of CNCs in the PEG matrix.

Keywords: cellulose nanocrystals, polyethylene glycol, apparent yield stress, percolation network

1. Introduction

Over the last decades, the interest for carbon [1,2], clay [3] and cellulosic [4] nanoparticle-based composites has been growing. Due to their natural abundance, biodegradability, optical properties, high stiffness and low density [5,6], cellulose nanocrystals (CNCs) have a potential for the reinforcement of thermoplastic matrices [7]. Polar CNCs are usually produced by sulfuric acid hydrolysis of wood pulp [8], followed by freeze-drying or spray-drying [9]. These drying processes, essential to store and commercialize CNCs [6], cause a strong agglomeration [10], which are then difficult to redisperse using conventional melt mixing methods, especially in non-polar thermoplastics [11]. Despite higher costs, solution mixing allows for well-dispersed nanocomposites [12–17] and could potentially be performed directly during the aqueous hydrolysis phase. The structure of CNCs in various media is still misunderstood. Agglomerates can be broken by the ultrasonication of CNC aqueous suspensions to achieve nanodispersion [18].

Polyethylene oxide (PEO) or glycol (PEG) (depending on molar weight) is a water-soluble biocompatible polymer used in biomedical applications [19]. Since it has a low melting point [20,21], CNC thermal degradation can be avoided when preparing composites in the molten state [22]. In fact, PEG/CNC may be considered as a model system to improve our knowledge of the behavior of CNCs in the presence of polymers [23], from aqueous suspensions to composites. The development of thermodynamic, structural and rheological methods for optimal dispersion of CNCs will be useful for future CNC applications. Moreover, the role of PEG in CNC colloidal aqueous suspensions is very important for hydrogel production [24] or fiber electrospinning [25]. Previous studies showed that PEG did not adsorb on cellulosic fibers [26] or microcrystals [27]. However, while some authors suggest the adsorption of PEG on CNC surfaces [28–30], their results seem to be incompatible with an adsorption mechanism [31,32]. Generally, polymer adsorption on CNC surfaces leads to a gelation at both low polymer and CNC concentrations, often associated with a bridging effect [31,33], while a slow flocculation by depletion is usually observed for non-adsorbed polymers [34]. The rheological behavior of CNC suspensions in polymeric media is controlled by the

morphology of nanoparticles and nanocomposite structure. Rheology is a useful tool to investigate the phenomena involved during the elaboration steps (from aqueous suspensions to molten composites).

The rheological properties of CNC water suspensions have been heavily investigated [18,35,36]. However, the rheological behavior of CNCs in thermoplastics [37], often prepared via solvent mixing, still needs clarification. Favier *et al.* [38] first showed a percolation network between tunicate CNCs that occurred at a critical volume fraction of 1 vol% in a styrene-butyl acrylate copolymer. Later, Tin *et al.* [39] observed a solid-like behavior at low frequencies for aqueous suspensions above 1 vol% of wood pulp CNCs in polyhydroxalkanoate (PHA). A yield stress related to a CNC percolation network was reported by Bagheriasl *et al.* [17] for polylactide (PLA)/CNC nanocomposites elaborated by solution mixing at concentrations above ~0.5 vol%. This network was correlated with an improvement of the mechanical properties of the composite [40]. Kamal and Khoshkava [41] obtained similar properties for PLA/2 vol% CNC composites prepared by melt mixing using a unique spray-freeze-drying process to prepare the CNCs. In another study, PEO was used as a compatibilizer in PLA/CNC nanocomposites to improve filler dispersion and decrease the percolation threshold [42]. Finally, Safdari *et al.* [43] have observed a yield behavior of PEO/cellulose nanofibers (CNFs) around 1 vol% CNFs, a value similar to that reported in the case of a PLA matrix [44].

The aim of this study is to understand via rheology the CNC structuration in the presence of a water-soluble, polar and Newtonian PEG thermoplastic matrix, from aqueous suspensions to composites, used as a model system. The influence of the CNC dispersion state in aqueous suspensions on the final rheological properties of the PEG/CNC composites is investigated for different ultrasonication treatments and two types of CNC (spray or freeze-dried sample). This fundamental step is helpful for the future understanding of new nanocomposites systems, elaborated by melt-mixing with thermoplastic matrices.

2. Materials and methods

Water-soluble polyethylene glycol (PEG) was purchased from Sigma Aldrich (Oakville, Ontario, Canada). From the technical data sheet the PEG density is 1.14 g.cm^{-3} , number average molar weight, M_n , is $\sim 20,000 \text{ g.mol}^{-1}$ and melting point, T_m , $\sim 63\text{-}66$ °C. Its polydispersity index is estimated to be 1.05, according polydispersity measurements done by Ling *et al.* [45] for several PEG grades supplied by Sigma Aldrich and Alfa Aesar (Tianjin, China).

CNCs obtained from sulfuric acid hydrolysis of wood pulp [8] followed by neutralization with sodium hydroxide (NaOH) and spray or freeze-drying processes were supplied by CelluForce (Montreal, Canada) and FPIInnovations (Pointe Claire, Canada), respectively. The presence of 3.4 sulfate half ester groups $\text{O-SO}_3\text{H}$ per 100 anhydroglucose units on CNC surfaces was determined by X-Ray spectroscopy (EDX) for both spray and freeze-dried CNCs, using a Tabletop Hitachi TM3030+ scanning electron microscope operating at 15 kV. The dimensions of the CNC particles were measured via transmission electronic microscopy (TEM) based on the measurements of at least 100 particles, using a TEM Jeol JEM 2100F bright field imaging, operating at 200 kV. The average length L_0 , diameter d_0 and aspect ratio p_0 were 165 nm, 13 nm and 12.5, respectively. The density of CNCs was taken equal to 1.54 g.cm^{-3} .

CNC suspensions with a volume fraction $\phi = 3.3 \text{ vol}\%$ in Milli-Q water (at $18.2 \text{ M}\Omega\text{.cm}$) were ultrasonicated using a Sonics & Materials VCX500 probe, operating at 20 kHz, using two different power levels P (10 and 50 W), and energy E varying from 5,000 to 10,000 J/g_{CNC}. The volume in the glass container used was $\sim 40 \text{ mL}$ (2.9 cm height by 2.1 cm radius). The container was placed in an ice bath and the ultrasonication was applied in pulse cycles: 10 s ON / 1 s OFF for $P = 10 \text{ W}$, and of 1 s ON / 1 s OFF for $P = 50 \text{ W}$, in order to avoid overheating. The intensity weighted mean hydrodynamic diameter (Z -average) of the CNC particles in suspensions was measured for dilute suspensions (0.03, 0.6 and 0.13 vol%) by diffusion light scattering (DLS), using a Malvern Zetasizer Nano-ZS (DTS1070 cell). The average results are reported in Table I. The higher Z -average values for low ultrasonication treatments were mainly attributed to the presence of some large CNC agglomerates with a size of few micrometers,

particularly observed in the case of freeze-dried CNC. However, most particles had a mean hydrodynamic diameter of few tenths of nanometers. The same limit particle size was reached for both spray and freeze-dried CNCs, after an efficient ultrasonication treatment.

TABLE I. Z-average hydrodynamic diameters for CNC aqueous suspensions after different ultrasonication treatments.

CNC	Power (W)	Energy (J/g _{CNC})	Z-average diameter (nm)
Spray-dried	10	5,000	115
		10,000	75
	50	10,000	75
Freeze-dried	10	5,000	145
	50	10,000	75

PEG flakes were solubilized in Milli-Q water for 30 min at 400 rpm under magnetic stirring at 50 °C. Then, the CNC suspensions were mixed using a magnetic stirrer for 30 min at 400 rpm at room temperature with PEG aqueous solutions to obtain suspensions with a final CNC volume fraction ϕ ranging from 0 to 2 vol% and containing 0, 20, 30 and 40 wt% PEG with respect to water and PEG. Finally, to obtain PEG composites with CNC concentrations ranging from 0 to 3.8 vol%, samples were dried under vacuum at $T = 50$ °C for 48 h and compression molded at 80 °C for 10 min using a Carver hydraulic press, in order to obtain disk-shaped samples for rheometry. The pressure was increased by steps from 0 to 27.6 MPa in order to avoid air bubbles, and the samples were cooled down to room temperature using a water cooling system.

Potential PEG adsorption on CNC was investigated following the method proposed by Lenfant *et al.* [31] in the case of hydroxyethyl cellulose (HEC). A Cannon Fenske viscometer with a capillary diameter of 50 μm was used. A calibration curve of the PEG solution relative viscosity η_r as a function of polymer initial concentration c_i is plotted, at $T = 25^\circ\text{C}$, in Fig. 1. The solution flow times are ranging from 195 to 305 s for Milli-Q water and $c_i = 0.01 \text{ g.mL}^{-1}$ PEG solution, respectively. The data were fitted using the Kraemer equation [46]:

$$\ln \eta_r = [\eta]c_i + (k_H - \frac{1}{2})[\eta]^2 c_i^2 \quad (1)$$

where $[\eta]$ is the intrinsic viscosity and the Huggins constant $k_H = 0.54$ [47]. The intrinsic viscosity $[\eta]$ was determined to be $\sim 45 \text{ mL.g}^{-1}$ for PEG in water at $T = 25^\circ\text{C}$, similar to the value obtained by Shulyak *et al.* [48] and corresponding to $c^* \sim 1/[\eta] \sim 0.022 \text{ g.mL}^{-1}$, which characterizes the limiting concentration for the dilute regime. The Mark–Houwink relation $[\eta] = K_\eta M_v^\alpha$ was used to determine the viscosity-average molar weight $M_v \sim 23,000 \text{ g.mol}^{-1}$, considering $K_\eta = 4.40 \times 10^{-2} \text{ mL.g}^{-1}$ and $\alpha = 0.69$ [48], close to the number average molar weight M_n given by the supplier ($20,000 \text{ g.mol}^{-1}$).

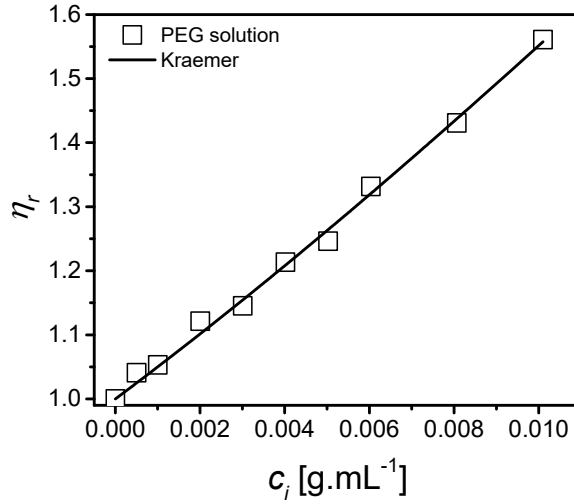


FIG. 1. Relative viscosity η_r as function of concentration c_i for water/PEG solutions. The line corresponds to the fit of the Kraemer equation.

A spray-dried CNC suspension with $\phi = 3.3 \text{ vol}\%$ was ultrasonicated at $P = 50 \text{ W}$ and $E = 10,000 \text{ J/g}_{\text{CNC}}$. Then, sixteen (16) suspensions were prepared as described previously with a CNC volume fraction ϕ ranging from 0 to 0.65 vol% and PEG concentration c_i ranging from 0.005 to 0.01 g.mL $^{-1}$ and corresponding to the dilute regime. The suspensions were allowed to rest at room temperature for 24 h. Then, CaCl $_2$ up to a concentration of 100 mM was added to the suspensions in order to precipitate the CNCs and trap the adsorbed polymer chains, with the assumption that the salt addition does not disturb the polymer adsorption phenomenon [31]. The suspensions were then centrifuged for 20 min at 13,000 rpm. We note that the centrifugation of CNC

suspensions without CaCl₂ addition did not allow for phase separation. Finally, the supernatant containing the non-adsorbed PEG was extracted and its flow time was measured using a Cannon Fenske viscometer to determine the final polymer concentration, c_f , using the calibration curve (Fig. 1). The adsorbed PEG concentration $c_i - c_f$ was determined and converted into Γ_{ads} as mg of adsorbed PEG per g of CNC.

For CNC suspensions in aqueous PEG solutions, the rheological tests were performed using a controlled stress Anton Paar MCR502 rheometer (equipped with a double-wall Couette geometry), after a pre-shear at 100 s⁻¹ over 100 s followed by a rest time of 180 s, to obtain a comparable initial state. Frequency sweep tests, with frequency ω ranging from 100 to 10⁻² rad.s⁻¹, at a strain amplitude γ within the linear viscoelastic regime, and shear rate tests, $\dot{\gamma}$ ranging from 0.5 s⁻¹ 500 s⁻¹, were performed. Time sweep measurements in the linear domain were done at $\omega = 5$ rad.s⁻¹ for CNC suspensions in aqueous PEG solutions with $\phi = 2$ vol% for 10 h.

For PEG/CNC composites, oscillatory shear measurements were performed on disk shape samples dried under vacuum for 24 h at $T = 50^\circ\text{C}$ using a controlled stress Anton Paar MCR301 rheometer equipped with a parallel plate geometry with a diameter of 25 mm and a gap of 1 mm. The rheological tests were carried out under air, in the molten state at 80 °C, for spray and freeze-dried CNC-based PEG composites with a CNC volume fraction ϕ ranging from 0 to 3.8 vol%, previously ultrasonicated following different treatments (Table I). Time sweep measurement showed that the viscoelastic properties of PEG and PEG/CNC composites ($\phi = 3.8$ vol%) were stable at $T = 80^\circ\text{C}$ for 4 h (results not shown). Strain sweep tests, with strain amplitude γ ranging from 0.0001 to 1, at $\omega = 10$ rad.s⁻¹ and frequency sweep tests, ω ranging from 100 to 10⁻² rad.s⁻¹, in the linear domain, were conducted at $T = 80^\circ\text{C}$ without pre-shearing to preserve the initial CNC structure. All rheological data were reproducible to $\pm 10\%$.

TEM images of CNC in the PEG matrix were taken using a bright field imaging Jeol JEM 2100F, operating at 200 kV. Because the crumbling characteristics of PEG/CNC composites did not allow the use of an ultracryomicrotome after compression

molding, the initial CNC suspension with $\phi = 0.07$ vol% CNCs (or 0.2 vol% relative to PEG) and 40 wt% PEG was diluted one hundred times with Milli-Q water, in order to obtain a thin film of PEG/CNC composite. A droplet of this suspension was dried to eliminate water, at room temperature on TEM grids for 30 min before observation. Fig. 2 presents the TEM image of that PEG/0.2 vol% spray-dried CNC nanocomposite initially ultrasonicated at $P = 50$ W and $E = 10,000$ J/g_{CNC}. This image shows the percolation between CNC nanoparticles, at this concentration ($\phi \sim 0.2$ vol%), in micron size flocs (ξ , drawn as illustrative) usually observed in the case of colloidal gels [49].

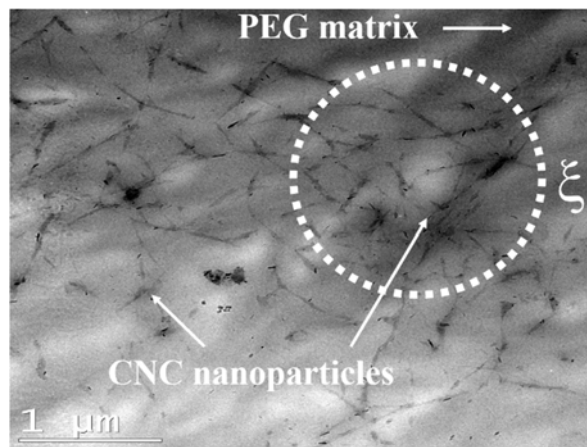


FIG. 2. TEM image of a PEG/0.2 vol% spray-dried CNC nanocomposite.

3. Results and discussion

3.1 Role of PEG in CNC aqueous suspensions

In this part concerning the role of PEG in CNC aqueous suspension, the tests were carried out after the ultrasonication of spray-dried CNC water suspension at $P = 50$ W and $E = 10,000$ J/g_{CNC}.

The possible adsorption phenomenon of PEG on CNC surface is compared to that observed by Lenfant *et al.* for HEC [31]. The theoretical maximum adsorption of PEG on

CNC surface, $\Gamma_{ads\ max} \sim 250$ mg/g, was estimated using the relation proposed by van de Ven [50], based on geometrical parameters of PEG chains and CNC surface:

$$\Gamma_{ads\ max} = k_c \frac{M_v}{N_A} \frac{A}{\pi a^2} \quad (2)$$

where $k_c = 0.55$ for random coverage, $M_v = 23,000$ g.mol⁻¹ is the viscosity-average molar weight (calculated from the relative viscosity, Fig. 1), N_A the Avogadro number (M_v/N_A represents the mass of a single polymer chain), $A = 250$ m²/g [51], the specific surface area of CNCs, and $a = a(N/6)^{1/2}$, the gyration radius of PEG chains for which the monomer length is $a = 0.297$ nm, and the degree of polymerization $N \sim 450$. In the case of HEC, this relation gives $\Gamma_{ads\ max} \sim 300$ mg/g, in the same order of magnitude as the maximum adsorption plateau value measured by viscometry, *i.e.* $\Gamma_{ads\ max} \sim 400$ mg/g [31].

Fig. 3 presents the adsorption isotherms of PEG and HEC on CNCs, Γ_{ads} , as a function of the final polymer concentration, c_f . For all PEG samples Γ_{ads} is close to 0, very far from the estimated value of 250 mg/g based on Eq. (2), suggesting that PEG chains do not adsorb on CNC surface (assuming that the salt addition did not induce polymer desorption [31]) and confirming the results of a recent study [52]. As reported by Reid *et al.* [32] the potential hydrogen bonding between the polymer and CNCs does not govern the adsorption in water, in disagreement with Cheng *et al.*'s [29] suggestion. However, HEC adsorption was clearly demonstrated by Lenfant *et al.* [31] (Fig. 3).

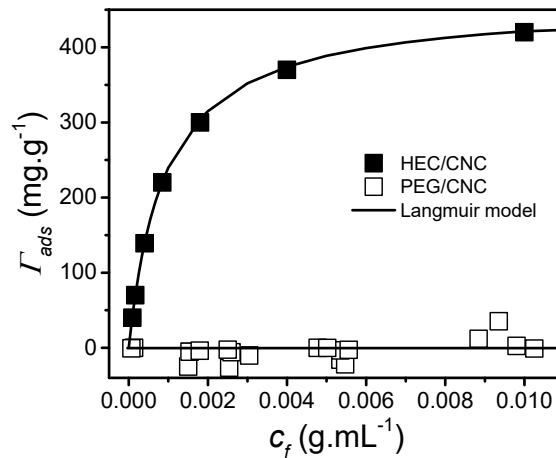


FIG. 3. Isotherm adsorptions Γ_{ads} as function of the concentration c_f for PEG and HEC (data of Lenfant *et al.* [31]). Lines correspond to the Langmuir model fits [53] and no adsorption is seen for PEG.

Non-ionic polymer adsorption on fillers can also be predicted by considering successively the solvent or polymer affinity towards the two other phases. Thermodynamically, polymer adsorption is possible when the entropy loss related to changes in the polymer chain conformation is lower than the enthalpy gain by the system caused by heat release [26]. In other words, polymer adsorption can occur if the affinity between the polymer chains and the filler surface is higher than that between the solvent and the filler surface. We use the method proposed by Sumita *et al.* [54], widely used in the case of ternary thermoplastic nanocomposites [55], to predict the filler location in emulsions. The first step of the Sumita *et al.* method considers the dispersive γ^d and polar γ^p components of the surface tensions γ to determine the interfacial tension between two compounds (1 and 2) using the Wu's harmonic mean average equation [56]:

$$\gamma_{1-2} = \gamma_1 + \gamma_2 - 2\sqrt{\gamma_1^d \gamma_2^d} - 2\sqrt{\gamma_1^p \gamma_2^p} \quad (3)$$

Using these interfacial tensions, the wetting coefficient ω_a can be determined to quantify the affinity of one component, called C , towards two others called A and B :

$$\omega_a = \frac{\gamma_{C-B} - \gamma_{C-A}}{\gamma_{A-B}} \quad (4)$$

If $-1 < \omega_a < 1$, the component C is preferentially located at the interface between A and B while when $\omega_a < -1$ and $\omega_a > 1$, the affinity of C towards B or A is larger, respectively. An adsorption parameter X can be estimated from the difference between the wetting coefficient of C with the solvent ω_{aS} , and that with the polymer, ω_{aP} (for $X > 0$, the affinity between the polymer and the filler surface is higher than that between the solvent and the filler surface). Table II presents the dispersive γ^d and polar γ^p contributions of the surface tensions γ , of water, polyethylene glycol (PEG), hydroxyethyl cellulose (HEC) and CNC taken from the literature. Using Eq. (3), the interfacial tensions $\gamma_{\text{water-PEG}}$, $\gamma_{\text{water-CNC}}$ and $\gamma_{\text{PEG-CNC}}$ are respectively equal to 14.06, 6.40 and 3.98 mJ.m⁻², leading to $\omega_{aS} = -1.92$ and $\omega_{aP} = -1.57$ for PEG (Eq. (4)). The adsorption parameter $X = -0.35$ (< 0), suggests that the PEG chain adsorption on CNCs seems not to be favored thermodynamically. For HEC, same calculation leads to $X = 1.96$ (> 0),

suggesting a possible polymer adsorption on CNC surface. These results confirm that PEG would not adsorb on CNC surface, whereas adsorption would be important in the case of HEC. Let us note that using the surface tension of polyvinyl alcohol (PVA) [57] and dextran [58], this approach predicts their respective adsorption and non-adsorption on CNCs, in agreement with demonstrations in the literature [33,59].

TABLE II. Dispersive γ^d and polar γ^p components of the surface tensions γ of components at room temperature.

	γ^d (mJ/m ²)	γ^p (mJ/m ²)	γ (mJ/m ²)
Water [60]	21.8	51.0	72.8
PEG [61]	30.6	12.2	42.8
HEC [62]	25.6	36.9	62.5
CNC [51]	40.9	28.0	68.9

Fig. 4 presents the variation of the elastic G' and loss G'' moduli as functions of time for the spray-dried CNC suspensions without and with the addition of 20, 30 and 40 wt% PEG in water for CNC $\phi = 2$ vol%, in the linear domain over 10 h.

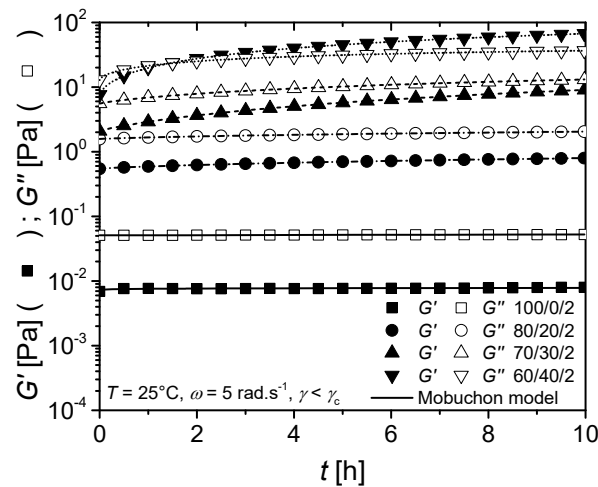


FIG. 4. Time sweeps for water/PEG/CNC suspensions with $\phi = 2$ vol%. Lines correspond to the Mobuchon model fits [63].

For the suspensions in the PEG solutions, we observed increases of the moduli over time. These increases can be described by the empirical model proposed by Mobuchon *et al.* [63], adapted from Dullaert and Mewis [64]:

$$G'(t) = G'_i + (G'_\infty - G'_i) \left(1 - \exp \left[- \left(\frac{t}{\tau'_b} \right)^m \right] \right) \quad (5)$$

where G'_i , G'_∞ are respectively the initial and final storage modulus at $t = 0$ and t tending towards infinity, and τ'_b and m are a characteristic time of the structure build-up and a stretching exponent, respectively. The same equation (Eq. (5)) was used for the loss modulus G'' and taking the stretching exponent equal to 1 (a value close to 1 was obtained for all suspensions leaving this parameter free in a first fit, according to the same overall shape of time sweeps), the values for τ'_b , τ''_b , G'_∞ and G''_∞ obtained by the best fits of the curves of Fig. 4 are given in Table III. The increases of G' and G'' as functions of time are larger as the PEG concentration increases. A cross-over point between G' and G'' is clearly observed after about 1 h for the aqueous suspension containing 40 wt% PEG ($\phi = 2$ vol%), and G'_∞ is larger than G''_∞ (Table III), suggesting a gel structure. For the lower PEG concentrations ($\phi = 2$ vol%), $G'_\infty < G''_\infty$ but the difference between these two values is reduced as the PEG concentration increases. The characteristic times τ'_b and τ''_b decrease overall, respectively from ~ 41 h to ~ 10 h and from 89 h to 4 h, by increasing PEG concentration from 0 to 40 wt%, suggesting that PEG accelerates CNC structuration by favoring percolation. These characteristic times should be identical for G' and G'' but due to the empirical nature of this model these values need to be discussed with caution. The non-adsorbed PEG chains reduce the electrostatic repulsion due to depletion forces and a structure built-up occurs by flocculation, as reported by Lenfant *et al.* [65] in the case of an electrostatic repulsion screening by sodium chloride. Moreover, the excluded volume caused by PEG chains probably reduces the distance between CNCs by steric effect.

TABLE III. Fitted parameters τ'_b , τ''_b , G'_∞ and G''_∞ , for CNC suspensions at $\phi = 2$ vol%.

Water/PEG/CNC suspensions	τ'_b (h)	G'_∞ (Pa)	τ''_b (h)	G''_∞ (Pa)
100/0/2	41	0.009	89	0.06
80/20/2	12	0.97	10	2.3
70/30/2	15	16	11	18
60/40/2	10	98	4	37

In order to understand the role of PEG in the first minutes of the composite preparation, viscoelastic properties of the suspensions were measured directly after solution mixing, without excluding a variation of the rheological properties during the maximum 30 minutes of each test (Fig. 4), especially for highly concentrated systems in both PEG (30 and 40 wt%) and CNC (2 vol%). Fig. 5 presents the elastic G' and loss G'' moduli (a and c) and the complex η^* and shear η viscosities (b and d) as functions of angular frequency ω or shear rate $\dot{\gamma}$ for spray-dried CNC suspensions, without (a and b) and with the addition of 30 wt% PEG (c and d) in water for ϕ ranging from 0 to 2 vol%. No significant elastic modulus could be measured in the case of CNC water suspensions (Fig. 5(a)), and for all CNC polymeric suspensions (Fig. 5(c)), G'' is higher than G' , characterizing a liquid-like behavior. The addition of PEG and CNC increases the viscoelastic properties of suspensions. Except for the suspension containing 30 wt% PEG and 2 vol% CNC, where a strong structure builds-up, G' and G'' exhibit, respectively, a slope of 1 and 2 in the terminal zone, in agreement with the Newtonian plateau shown in Figs. 5(b) and 5(d). The Cox-Merz rule $\eta^*(\omega) = \eta(\dot{\gamma})$ is valid for all suspensions in Fig. 5, suggesting a weak structure [18]. At high frequencies and shear rates, shear thinning is observed above a critical shear rate $\dot{\gamma}_c$ (Fig. 5(b) and 5(d)), due to the orientation of CNCs in the flow direction, corresponding to the rotational Péclet number [66], $Pe_{rot} = 1$, characterizing the limit of the flow being dominated by Brownian motion and hydrodynamic forces. The critical shear rate $\dot{\gamma}_c$ decreases as the PEG concentration increases, due to the increase of the solution viscosity. At low frequencies and shear rates, a Newtonian plateau η_0 is observed for all suspensions. This result suggests that there is no polymer adsorption and bridging effect between CNCs, contrary to the fast gelation highlighted in the case of adsorbed polymers [31,33] at very low concentrations

of both CNC and polymer (~ 0.2 wt%), and in agreement with the adsorption isotherms of Fig. 3. Oguzlu and Boluk [30] did not observe CNC gelation with the addition of polyethylene oxide (PEO) in aqueous suspensions, but nevertheless attributed the increased rheological properties to PEO adsorbed on CNCs, which would increase steric repulsion between CNCs. However, a conventional colloidal electrostatic stability of CNC aqueous suspensions containing non-adsorbed polymer would seem a more appropriate mechanism.

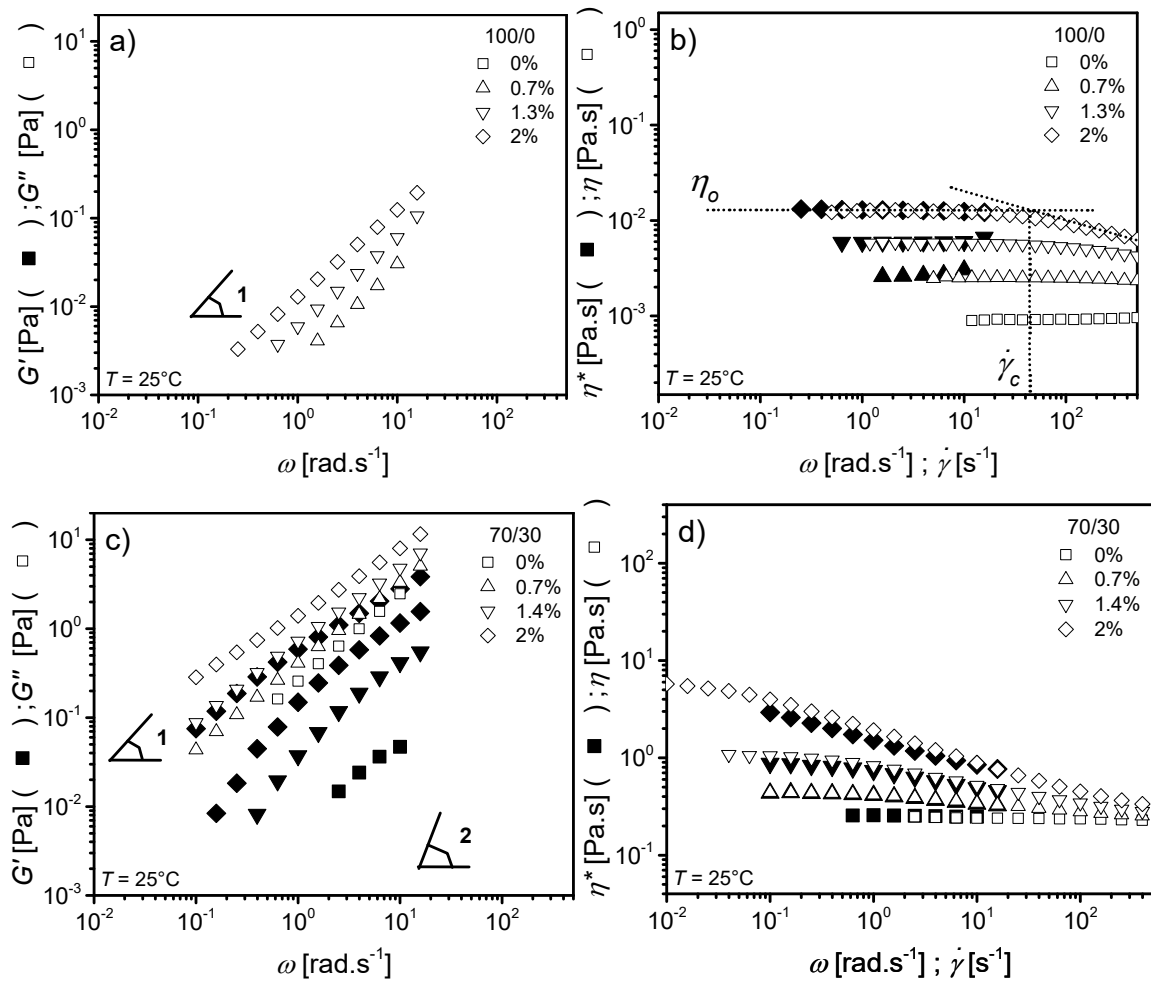


FIG. 5. Elastic G' (filled symbols) and loss G'' (open symbols) moduli (a, c), complex η^* (filled symbols) and shear η (open symbols) viscosities (b, d) as functions of angular frequency ω and shear rate $\dot{\gamma}$ for spray-dried CNC suspensions without PEG (a, b) and with 30 wt% (c, d) in water.

For all spray-dried CNC suspensions, without and with the addition of 20, 30 and 40 wt% PEG in water, the relative viscosity η_r is plotted as a function of CNC volume fraction ϕ in Fig. 6. The relative viscosity is defined as the ratio of the Newtonian viscosity of the filled suspension to that of the unfilled suspending medium,

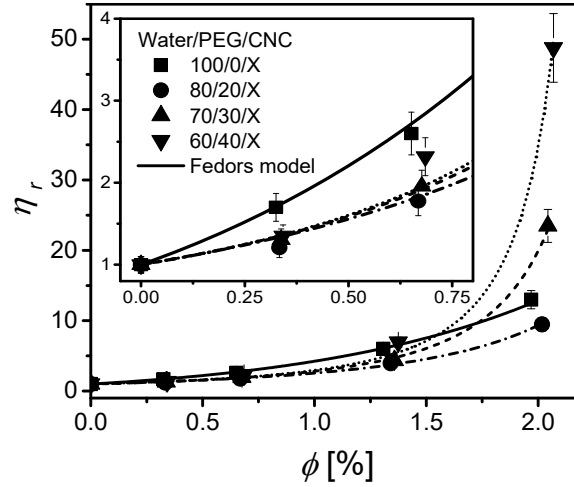


FIG. 6. Relative viscosity η_r as a function of volume fraction for the CNC suspensions in PEG aqueous solutions. Lines correspond to the Fedors model fits.

The Fedors model [67], widely used in the case of dilute and semi-dilute CNC suspensions [68], has been used to fit the experimental data of Fig. 6. It is expressed by:

$$\frac{1}{2(\sqrt{\eta_r} - 1)} = \frac{1}{\phi[\eta]} - \frac{1}{\phi_m[\eta]} \quad (6)$$

In the literature ϕ_m is usually called maximum packing density or fraction [35]; it is the concentration at which jamming occurs. The theoretical maximum packing fraction was estimated for rigid, non-interactive hexagonally packed cylindrical rods to be close to 90 vol% [69], which is much larger than the maximum packing fractions reported in Table IV. $[\eta]$ is the intrinsic viscosity, which is equal to the sum of the rigid body $[\eta]_o$ and the electroviscous $[\eta]_{el}$ contributions of CNC particles [68]. The Simha relation [70] validated for CNC nanorods [36] is used to determine the rigid body contribution:

$$[\eta]_0 = \frac{14}{15} + \frac{p^2}{15(\ln 2p - 1.5)} + \frac{p^2}{5(\ln 2p - 0.5)} \quad (7)$$

Taking the aspect ratio $p = 12.5$ as previously determined by TEM, $[\eta]_0 = 18.5$. The values of ϕ_m , $[\eta]$, $[\eta]_0$ and $[\eta]_{el}$ are listed in Table IV for all suspensions. As expected, η_r increases with ϕ up to a maximum volume fraction ϕ_m where η_r tends towards infinity. When the viscoelastic properties are quasi-independent of time, *i.e.* for low CNC concentrations, the addition of PEG leads to a less intense increase of η_r at low ϕ (insert Fig. 6), due to less electrostatic repulsion between CNCs, highlighted by the decrease of $[\eta]_{el}$ (Table 4). On the other hand, ϕ_m decreases with PEG concentration, suggesting that the PEG favors gelation between CNCs due to a depletion effect.

TABLE IV. Maximum packing volume fraction ϕ_m , intrinsic viscosity $[\eta]$ and its rigid body $[\eta]_0$ and electroviscous $[\eta]_{el}$ contributions for water/PEG/CNC suspensions.

Water/PEG/CNC suspensions	ϕ_m (vol%)	$[\eta]$	$[\eta]_0$	$[\eta]_{el}$
100/0/x	6.5	180	18.5	161.5
80/20/x	3.4	85		66.5
70/30/x	2.7			
60/40/x	2.4			

3.2 CNC network characterization in PEG thermoplastic matrix

In this section, the rheological behavior of PEG/spray and freeze-dried CNC nanocomposites is investigated, for different ultrasonication treatments of the precursor CNC aqueous suspensions (Table I), in order to develop rheological tools for indirect structural characterization of CNC composites based on molten polymers. Fig. 7 presents, as an example, a strain sweep test for the 2.2 vol% spray-dried CNCs in molten PEG at 80 °C, after an initial ultrasonication of the CNC aqueous suspension at $P = 50$ W and $E = 10,000$ J/g_{CNC}. Galindo-Rosales *et al.* [71] demonstrated that, above the percolation threshold, the ratio between the elastic modulus plateau G'_p and the maximum loss modulus value G''_{max} can be used as a criterion for the dispersion quality of the sample. This ratio characterizes the strength of the network at rest [72]. Even if for freeze-dried

and spray-dried CNC, both G'_p and G''_{max} are generally larger after a strong ultrasonication treatment ($E = 10,000 \text{ J/g}_{\text{CNC}}$) than those after a weak ultrasonication treatment ($E = 5,000 \text{ J/g}_{\text{CNC}}$), in agreement with the Z-average hydrodynamic diameter measurements (Table I), the ratio G'_p/G''_{max} is similar for each fraction (for example, close to 3.5 for $\phi = 2.2 \text{ vol\%}$), *i.e.* unchanged by the severity of the ultrasonic treatment, which clearly affects the dispersion of the CNCs. If the plateau values at low strains (G'_p and G''_p) were related to the floc network reorganization before rupture, G''_{max} was associated to conformation changes of agglomerates [73]. The strong interactions linking the CNC particles in agglomerates could prevent their rearrangement and could not discriminate the dispersion state refinement obtained after breaking agglomerates. Hence, the method proposed by Rosales *et al.* [71] is not conclusive to differentiate the dispersion quality of our PEG/CNC systems containing only a few large agglomerates.

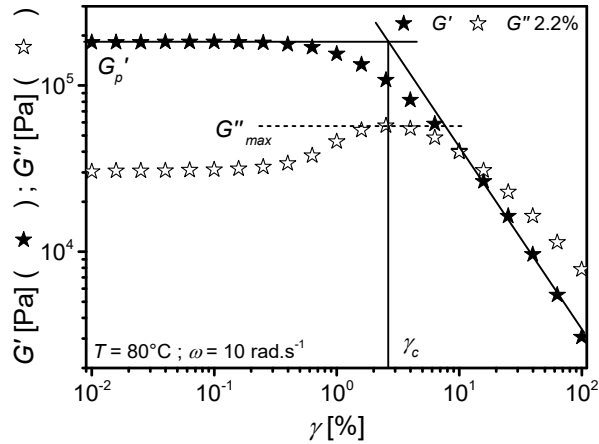


FIG. 7. Elastic G' (filled symbols) and loss G'' (open symbols) moduli as a function of strain γ for a PEG/2.2 vol% spray-dried CNC nanocomposite.

It is also possible to consider the critical strain and the apparent yield stress as criteria for the dispersion state of CNC in PEG. Strain sweep measurements were used to plot the variations of the critical strain γ_c , determined by the tangent method (as shown in Fig. 7) for the elastic modulus G' , as a function of volume fraction ϕ for PEG/spray-dried and freeze-dried CNC nanocomposites (Fig. 8). The critical strain values γ_c are about independent of the CNC used (spray-dried or freeze-dried) and the ultrasonication treatment applied within the range studied. We note that the determination of precise γ_c

values is difficult to highlight the different dispersion states of CNCs in PEG following ultrasonication treatments. For all nanocomposites, γ_c decreases with the volume fraction ϕ , following a power-law expression with an exponent equal to -0.8 ($\gamma_c \propto \phi^{-0.8}$). A slope of -2 was determined from Kamal and Khoshkava's data [41] for PLA/CNC composites prepared by melt mixing. In the case of polyamide composites filled with mineral platelets, a slope of -2 was measured for micrometric talc [74] while a slope of -1 was reported for nanometric organically modified montmorillonite [74,75], hinting at the nanodispersion of CNCs in PEG-based composites elaborated by solution mixing. Moreover, such viscoelastic non-linearities (Fig. 8) appear at lower volume fractions than those reported in the literature for PLA [40]. These results could be explained by the particle relative degree of dispersion state in the thermoplastic matrix, along with the affinity between CNC and the polymer, as observed by Beuguel *et al.* [74] in the case of PA/clay microcomposites and nanocomposites (with different values for the PA polarity and particle aspect ratio).

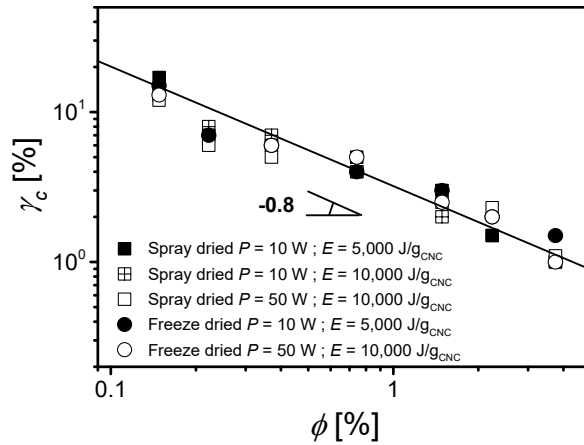


FIG. 8. Critical strain γ_c as a function of volume fraction for PEG/spray-dried and freeze-dried CNC nanocomposites.

Fig. 9 presents the variations of the elastic G' (a) and loss G'' (b) moduli as functions of angular frequency, in the linear viscoelastic domain $\gamma < \gamma_c$, for various contents of spray-dried CNCs in nanocomposites, initially sonicated at $P = 50$ W and $E = 10,000$ J/g_{CNC}. The behavior of other samples is similar. The elastic G' and loss G'' moduli are a quadratic and linear functions of angular frequency for the PEG Newtonian

matrix, respectively. For $\phi \geq 0.15$ vol%, the rheological behavior of PEG/CNC nanocomposites shows an elastic plateau modulus G'_0 , higher than the loss modulus G''_0 , indicating a gel behavior attributed to the percolation network between CNC, as observed in Fig. 2. These plateau moduli increase of about 3 decades for a volume fraction up to 3.8 vol%.

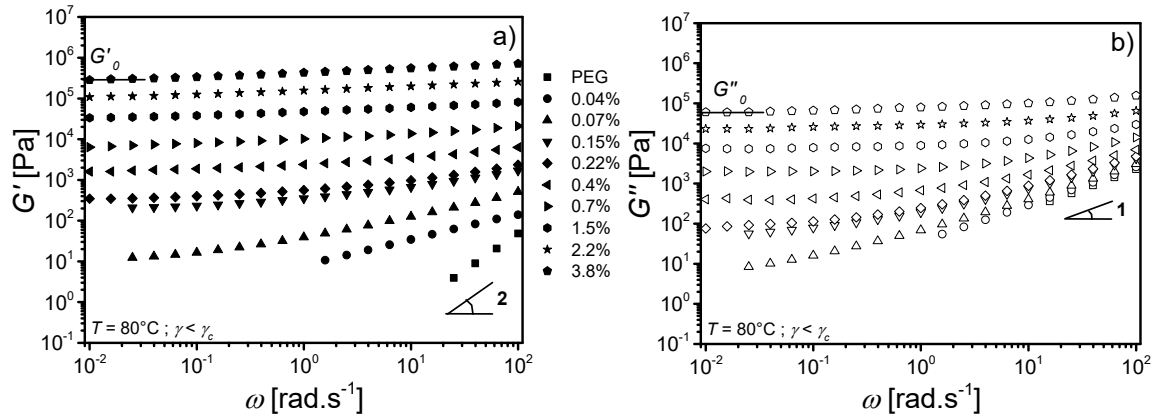


FIG. 9. Elastic G' (a, filled symbols) and loss G'' (b, open symbols) moduli as functions of angular frequency ω for PEG/spray-dried CNC nanocomposites.

Figs. 10(a) and 10(b) report the complex viscosity η^* as a function of the complex modulus G^* , in linear domain $\gamma < \gamma_c$, for PEG/spray-dried (a) and freeze-dried CNC (b) nanocomposites after different initial ultrasonication treatments.

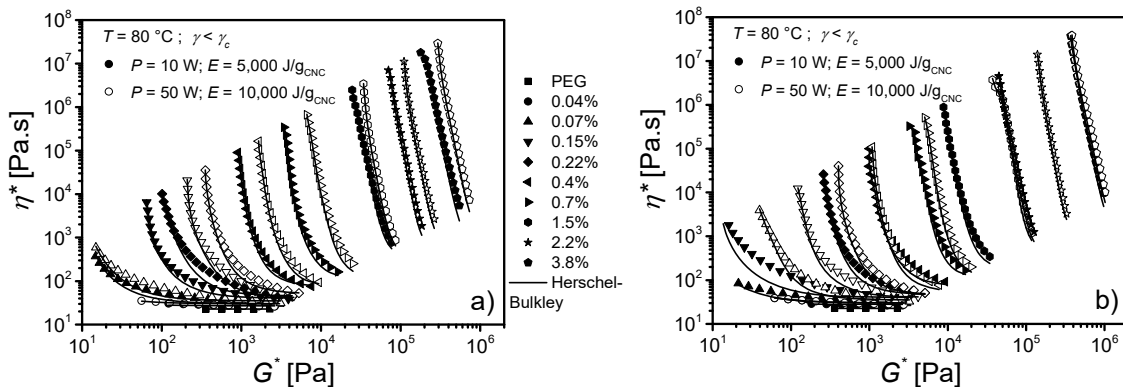


FIG. 10. Complex viscosity η^* as a function of complex modulus G^* for PEG/spray-dried (a) and freeze-dried (b) CNC nanocomposites. Filled symbols represent data for $P = 10$ W and open symbols those for $P = 50$ W; lines correspond to the Herschel-Bulkley model fits.

The experimental data are fitted with the modified Herschel-Bulkley model:

$$\eta^* = \frac{G_0^*}{\omega} + k(\gamma_0 \omega)^{n-1} \quad (8)$$

where the power-law index, n , was taken equal to 1 because PEG exhibits a Newtonian behavior over the entire frequency range studied (Fig. 9). Parameters G_0^* , ω , k and γ_0 are the complex modulus plateau at low frequencies, the angular frequency, the consistency index and the strain amplitude at which the tests were performed, respectively.

For an equivalent volume fraction ϕ , the data corresponding to nanocomposites obtained after a strong ultrasonication (open symbols) are overall above those measured after a weaker ultrasonication (filled symbols), for both spray and freeze-dried systems, in agreement with the Z -average hydrodynamic diameter measurements (Table I) and the presence of agglomerates at the lower ultrasonication energy ($E = 5,000 \text{ J/g}_{\text{CNC}}$). No significant apparent yield stress could be determined for suspensions containing less than 0.15 vol%, which corresponds to the percolation threshold (Fig. 2), ϕ_c . This value is considerably lower than those reported for PLA/CNC composites ($\phi_c \sim 0.5 - 2 \text{ vol\%}$) [17,41] or polycarbonate/carbon nanotubes (PC/CNT) ($\phi_c \sim 0.45$) [76]. Above ϕ_c , the percolated network induces a yield behavior at low frequencies, characterized by an apparent yield stress defined by $\tau_0^* = G_0^* \gamma_c$.

Fig. 11 presents the variation of the apparent yield stress τ_0^* as a function of volume fraction ϕ for PEG/spray-dried (a) and freeze-dried CNC (b) nanocomposites for different initial ultrasonication treatments. The solid and dotted lines are best fits of power-law expressions, $\tau_0^* \propto \phi^{1.8}$, for the ultrasonic treatment at 5,000 and 10,000 J/g_{CNC}, respectively. Overall, the apparent yield stress values τ_0^* are higher for the PEG/CNC nanocomposites prepared after a strong ultrasonication treatment ($E = 10,000 \text{ J/g}_{\text{CNC}}$), corresponding to well-dispersed systems. The presence of some remaining agglomerates for the lower ultrasonicated composites ($E = 5,000 \text{ J/g}_{\text{CNC}}$) shifts the curve towards higher volume fractions, especially for PEG/freeze-dried CNC containing larger agglomerates (Table I). The presence of agglomerates seems to delay, in terms of volume fraction ϕ ,

the percolation threshold. More specifically, we need to add 25% (Fig. 11(a)) and 50% (Fig. 11(b)) more CNCs, respectively, in the case of PEG/CNC spray and freeze-dried CNC containing agglomerates, to obtain a nanocomposite with an equivalent yield stress. The apparent yield stress values are similar for well dispersed spray-dried and freeze-dried CNC nanocomposites and τ_0^* increases as a function of ϕ with a power-law exponent n of 1.8, which is much smaller than the value of 6.3 reported by Kamal and Khoshkava [41] for PLA/CNC composites prepared by melt mixing. However, it is close to those calculated by Bagheriasl *et al.* [17] for PLA/CNC nanocomposites elaborated by solution mixing (exponent of 2.6), by Aubry *et al.* [75] and by Rahatekar *et al.* [77] (modeled by Bounoua *et al.* [78]) for PA/OMMT and epoxy/CNT nanocomposites, respectively (exponent of 2). Furthermore the percolation threshold, ϕ_c , is much smaller for PEG/CNC nanocomposites (~ 0.15 vol%) than for PLA/CNC nanocomposites (0.5 and 2 vol%) [17,41]. Beyond the probably better nanodispersion state achieved via a good solvent solution mixing method in water and an efficient ultrasonication treatment, this lower threshold could be partially explained by the better affinity between the matrix and the filler [72], as suggested by the lower interfacial tension $\gamma_{PEG-CNC} = 3.98$ mJ/m² (Eq. (3) and Table II) compared to $\gamma_{PLA-CNC} = 6.38$ mJ/m² (using the surface tension of PLA reported by Khoshkava [51]).

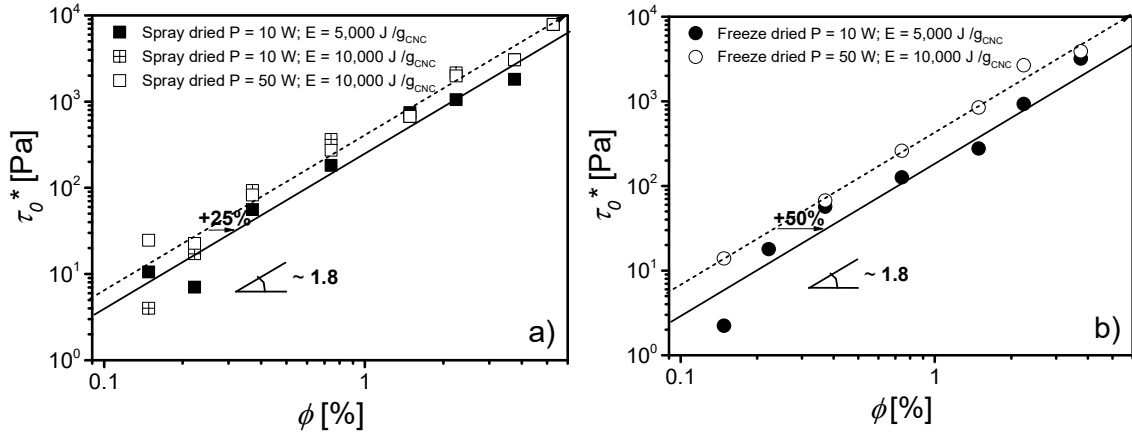


FIG. 11. Apparent yield stress τ_0^* as a function of volume fraction for PEG/spray-dried (a) and freeze-dried (b) CNC nanocomposites.

The elastic modulus at low frequencies G'_0 conveys similar information as the apparent yield stress τ_0^* . It is plotted as a function of volume fraction ϕ in Fig. 12 for PEG/spray-dried (a) and freeze-dried CNC (b) nanocomposites after different initial ultrasonication treatments. The elastic modulus plateau G'_0 follows a power-law expression with an exponent of 2.7 ($G'_0 \propto \phi^{2.7}$), similar to 2.6 obtained by Abbasi *et al.* [76] for well dispersed carbon nanotube (CNT) in polycarbonate (PC). As observed for the apparent yield stress τ_0^* , the presence of agglomerates decreases the elastic response of the nanocomposites by trapping a large amount of CNCs that apparently play no significant role on the percolated network structure.

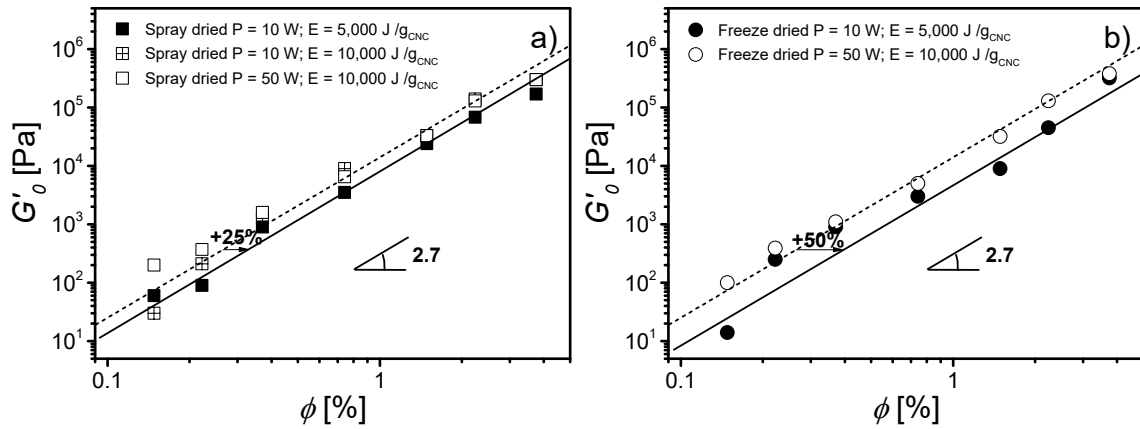


FIG. 12. Elastic modulus plateau G'_0 as a function of volume fraction ϕ for PEG/spray-dried (a) and freeze-dried (b) CNC nanocomposites.

Shih *et al.* [79] proposed a scaling model to determine the fractal dimensions of a colloidal gel floc structure d_f and of its backbone x . They considered an extremely strong-like gel where the interfloc links are stronger than the intrafloc ones, compared to an extremely weak-like regime where the intrafloc links are stronger than the interfloc ones. The fractal dimensions d_f and x are related to the power-law expression exponents for γ_c and G'_0 as a function of ϕ :

$$G'_0 = \phi^A \quad (9)$$

and
$$\gamma_c = \phi^B \quad (10)$$

where
$$A = (d + x)/(d - d_f) \quad (11)$$

and
$$B = -(1+x)/(d-d_f) \quad (12)$$

with the Euclidian dimension of the system, $d = 3$.

As reported above, $G'_0 \propto \phi^{2.7}$ and $\gamma_c \propto \phi^{-0.8}$ for the PEG/CNC nanocomposites. Hence, from Eqs. (10) – (13) the fractal dimension characterizing the floc structure is $d_f \sim 2$, suggesting a 2-D network (could be imagined as a layer network while it is often considered as 3-D), apparently observed in Fig. 2. This value is similar to those measured by small-angle neutron scattering in the case of CNC hydrogels [80]. It is worth pointing out that compression molding in the molten state of the PEG/CNC composites could modify the image obtained by TEM (Fig.2). However, x is equal to -0.15, which does not make any physical sense. Recently, Wu *et al.* [49] extended the Shih *et al.* model and defined a new parameter α attributed to a transition ($0 < \alpha < 1$) from extremely strong-like ($\alpha = 0$) to weak-like ($\alpha = 1$) gels:

$$A = \beta/(d-d_f) \quad (13)$$

and
$$B = (d-\beta-1)/(d-d_f) \quad (14)$$

where
$$\beta = (d-2) + (2+x)(1-\alpha) \quad (15)$$

They proposed setting the backbone fractal dimension x between 1 and 1.3, as usually reported for colloidal gels. This leads to the same fractal dimension $d_f \sim 2$ and the parameter $\alpha = 0.38 - 0.44$ for PEG/CNC nanocomposites, suggesting that the contribution of interfloc links is slightly more important. Finally, it is worth pointing out that the network characterization described above was performed for a compatible system prepared in favorable solution mixing conditions, and could be affected by the stress applied during subsequent compression molding. Results could be different in the case of composites based on conventional non-polar thermoplastic matrices and prepared from the melt state in extrusion or injection molding.

4 Conclusion

Our rheological data on suspensions of CNCs in aqueous solution of PEG suggest that PEG chains do not adsorb on CNCs. Gelation due to depletion forces is the most probable mechanism for aqueous suspensions containing relatively high concentrations of both PEG (40 wt%) and CNC (2 vol%). The intrinsic viscosity values of PEG/CNC aqueous suspensions highlight a decrease of electrostatic repulsion between CNCs with the addition of the polymer. After drying and compression molding, the PEG/CNC nanocomposites in the molten state show exceptional viscoelastic properties, characterized by apparent yield stress values beyond a percolation threshold volume fraction of 0.15 vol%, in agreement with the network observed by TEM at 0.2 vol%. The critical strain amplitude and the elastic plateau modulus follow, respectively, a power law with an exponent -0.8 and 2.7 as a function of volume fraction, close to the values reported in the literature for well dispersed nanocomposites. The presence of some agglomerates decreases the rheological properties and imposes to add more CNCs in order to obtain similar values (+ 50% in the worst dispersion case studied). However, the percolated network structure governing the rheological behavior is unaffected by the presence of these agglomerates. Finally, the Shih *et al.* model was used to determine a fractal dimension of 2, suggesting a 2D network of CNCs in the PEG matrix, mainly controlled by interfloc links. This work demonstrates the important potential of bio-based and biodegradable CNCs to reinforce thermoplastic matrices and improve their end-properties. The thermodynamic, structural and rheological tools developed in this work will be helpful for future CNC applications.

5 Acknowledgments

FPInnovations and CelluForce are acknowledged for providing the CNCs. We also thank FPInnovations, NSERC and PRIMA Québec for their financial support. The authors are grateful to Dr. Wadood Hamad of FPInnovations for his helpful suggestions. The authors thank Mr. Philippe Massé for his help with TEM observations. We are grateful to Prof. Daria Camilla Boffito for her help with ultrasonication, Prof. Nick

Virgilio and Prof. Theo van de Ven (U McGill) for their expertise in polymer adsorption and Dr. Gilles Lenfant for his inspiring discussions about rheology of CNC suspensions.

6 References

- [1] Thostenson, E. T., Z. Ren, and T.-W. Chou, “Advances in the science and technology of carbon nanotubes and their composites: a review,” *Compos. Sci. Technol.* **61**, 1899–1912 (2001).
- [2] Kim, H., A. A. Abdala, and C. W. Macosko, “Graphene/Polymer Nanocomposites,” *Macromolecules* **43**, 6515–6530 (2010).
- [3] Sinha Ray, S., and M. Okamoto, “Polymer/layered silicate nanocomposites: a review from preparation to processing,” *Prog. Polym. Sci.* **28**, 1539–1641 (2003).
- [4] Moon, R. J., A. Martini, J. Nairn, J. Simonsen, and J. Youngblood, “Cellulose nanomaterials review: structure, properties and nanocomposites,” *Chem. Soc. Rev.* **40**, 3941 (2011).
- [5] Habibi, Y., L. a Lucia, and O. J. Rojas, “Cellulose Nanocrystals: Chemistry, Self-Assembly, and Applications,” *Chem. Rev.* **110**, 3479–3500 (2010).
- [6] Hamad, W. Y., “Cellulose Nanocrystals” (John Wiley & Sons, Ltd, Chichester, UK, 2017)
- [7] Mariano, M., N. El Kissi, and A. Dufresne, “Cellulose nanocrystals and related nanocomposites: Review of some properties and challenges,” *J. Polym. Sci. Part B Polym. Phys.* **52**, 791–806 (2014).
- [8] Brinchi, L., F. Cotana, E. Fortunati, and J. M. Kenny, “Production of nanocrystalline cellulose from lignocellulosic biomass: Technology and applications,” *Carbohydr. Polym.* **94**, 154–169 (2013).
- [9] Beck, S., J. Bouchard, and R. Berry, “Dispersibility in Water of Dried Nanocrystalline Cellulose,” *Biomacromolecules* **13**, 1486–1494 (2012).
- [10] Khoshkava, V., and M. R. R. Kamal, “Effect of drying conditions on cellulose nanocrystal (CNC) agglomerate porosity and dispersibility in polymer nanocomposites,” *Powder Technol.* **261**, 288–298 (2014).
- [11] Sojoudiasli, H., M.-C. Heuzey, and P. J. Carreau, “Mechanical and morphological properties of cellulose nanocrystal-polypropylene composites,” *Polym. Compos.* **16**, 101–113 (2017).
- [12] Azizi Samir, M. A. S., F. Alloin, J.-Y. Sanchez, and A. Dufresne, “Cellulose nanocrystals reinforced poly(oxyethylene),” *Polymer* **45**, 4149–4157 (2004).
- [13] Ljungberg, N., J. Y. Cavallé, and L. Heux, “Nanocomposites of isotactic polypropylene reinforced with rod-like cellulose whiskers,” *Polymer* **47**, 6285–6292 (2006).
- [14] Roohani, M., Y. Habibi, N. M. Belgacem, G. Ebrahim, A. N. Karimi, and A. Dufresne, “Cellulose whiskers reinforced polyvinyl alcohol copolymers nanocomposites,” *Eur. Polym. J.* **44**, 2489–2498 (2008).
- [15] Kaboorani, A., B. Riedl, P. Blanchet, M. Fellin, O. Hosseinaei, and S. Wang, “Nanocrystalline cellulose (NCC): A renewable nano-material for polyvinyl acetate (PVA) adhesive,” *Eur. Polym. J.* **48**, 1829–1837 (2012).

- [16] Xu, X., H. Wang, L. Jiang, X. Wang, S. a Payne, J. Y. Zhu, and R. Li, "Comparison between Cellulose Nanocrystal and Cellulose Nanofibril Reinforced Poly(ethylene oxide) Nanofibers and Their Novel Shish-Kebab-Like Crystalline Structures," *Macromolecules* **47**, 3409–3416 (2014).
- [17] Bagheriasl, D., P. J. Carreau, B. Riedl, C. Dubois, and W. Y. Hamad, "Shear rheology of polylactide (PLA)–cellulose nanocrystal (CNC) nanocomposites," *Cellulose* **23**, 1885–1897 (2016).
- [18] Shafiei-Sabet, S., W. Y. Hamad, and S. G. Hatzikiriakos, "Rheology of Nanocrystalline Cellulose Aqueous Suspensions," *Langmuir* **28**, 17124–17133 (2012).
- [19] Harris, J. M., *Poly(Ethylene Glycol) Chemistry: Biotechnical and Biomedical Applications* (J. M. Harris, Ed., Springer US, Boston, MA, 1992).
- [20] Mark, J. E., *Polymer Data Handbook* (Oxford University Press, Inc., 1999).
- [21] Pielichowski, K., and K. Flejtuch, "Differential scanning calorimetry studies on poly(ethylene glycol) with different molecular weights for thermal energy storage materials," *Polym. Adv. Technol.* **13**, 690–696 (2002).
- [22] Wang, N., E. Ding, and R. Cheng, "Thermal degradation behaviors of spherical cellulose nanocrystals with sulfate groups," *Polymer* **48**, 3486–3493 (2007).
- [23] Gu, M., C. Jiang, D. Liu, N. Prempeh, and I. I. Smalyukh, "Cellulose Nanocrystal/Poly(ethylene glycol) Composite as an Iridescent Coating on Polymer Substrates: Structure-Color and Interface Adhesion," *ACS Appl. Mater. Interfaces* **8**, 32565–32573 (2016).
- [24] Liang, S., J. Wu, H. Tian, L. Zhang, and J. Xu, "High-Strength Cellulose/Poly(ethylene glycol) Gels," *ChemSusChem* **1**, 558–563 (2008).
- [25] Zhou, C., R. Chu, R. Wu, and Q. Wu, "Electrospun Polyethylene Oxide/Cellulose Nanocrystal Composite Nanofibrous Mats with Homogeneous and Heterogeneous Microstructures," *Biomacromolecules* **12**, 2617–2625 (2011).
- [26] van de Ven, T. G. M., "Kinetic aspects of polymer and polyelectrolyte adsorption on surfaces," *Adv. Colloid Interface Sci.* **48**, 121–140 (1994).
- [27] Gaudreault, R., T. G. M. van de Ven, and M. A. Whitehead, "Mechanisms of flocculation with poly(ethylene oxide) and novel cofactors," *Colloids Surfaces A Physicochem. Eng. Asp.* **268**, 131–146 (2005).
- [28] Ben Azouz, K., E. C. Ramires, W. Van den Fonteyne, N. El Kissi, and A. Dufresne, "Simple Method for the Melt Extrusion of a Cellulose Nanocrystal Reinforced Hydrophobic Polymer," *ACS Macro Lett.* **1**, 236–240 (2012).
- [29] Cheng, D., Y. Wen, L. Wang, X. An, X. Zhu, and Y. Ni, "Adsorption of polyethylene glycol (PEG) onto cellulose nano-crystals to improve its dispersity," *Carbohydr. Polym.* **123**, 157–163 (2015).
- [30] Oguzlu, H., and Y. Boluk, "Interactions between cellulose nanocrystals and anionic and neutral polymers in aqueous solutions," *Cellulose* **24**, 131–146 (Springer Netherlands, 2017).
- [31] Lenfant, G., M.-C. Heuzey, T. G. M. van de Ven, and P. J. Carreau, "Gelation of crystalline nanocellulose in the presence of hydroxyethyl cellulose," *Can. J. Chem. Eng.* (2017).
- [32] Reid, M. S., M. Villalobos, and E. D. Cranston, "The Role of Hydrogen Bonding in Non-Ionic Polymer Adsorption to Cellulose Nanocrystals and Silica Colloids,"

- Curr. Opin. Colloid Interface Sci. **29**, 76–82 (2017).
- [33] Chen, Y., C. Xu, J. Huang, D. Wu, and Q. Lv, “Rheological properties of nanocrystalline cellulose suspensions,” *Carbohydr. Polym.* **157**, 303–310 (2017).
- [34] Boluk, Y., L. Zhao, and V. Incani, “Dispersions of Nanocrystalline Cellulose in Aqueous Polymer Solutions: Structure Formation of Colloidal Rods,” *Langmuir* **28**, 6114–6123 (2012).
- [35] Bercea, M., and P. Navard, “Shear Dynamics of Aqueous Suspensions of Cellulose Whiskers,” *Macromolecules* **33**, 6011–6016 (2000).
- [36] Boluk, Y., R. Lahiji, L. Zhao, and M. T. McDermott, “Suspension viscosities and shape parameter of cellulose nanocrystals (CNC),” *Colloids Surfaces A Physicochem. Eng. Asp.* **377**, 297–303 (2011).
- [37] Ching, Y. C., M. Ershad Ali, L. C. Abdullah, K. W. Choo, Y. C. Kuan, S. J. Julaihi, C. H. Chuah, and N.-S. Liou, “Rheological properties of cellulose nanocrystal-embedded polymer composites: a review,” *Cellulose* **23**, 1011–1030 (2016).
- [38] Favier, V., H. Chanzy, and J. Y. Cavaille, “Polymer Nanocomposites Reinforced by Cellulose Whiskers,” *Macromolecules* **28**, 6365–6367 (1995).
- [39] Ten, E., D. F. Bahr, B. Li, L. Jiang, and M. P. Wolcott, “Effects of Cellulose Nanowhiskers on Mechanical, Dielectric, and Rheological Properties of Poly(3-hydroxybutyrate- co -3-hydroxyvalerate)/Cellulose Nanowhisiker Composites,” *Ind. Eng. Chem. Res.* **51**, 2941–2951 (2012).
- [40] Bagheriasl, D., P. J. Carreau, B. Riedl, and C. Dubois, “Enhanced properties of polylactide by incorporating cellulose nanocrystals,” *Polym. Compos.* **13** (2016).
- [41] Kamal, M. R., and V. Khoshkava, “Effect of cellulose nanocrystals (CNC) on rheological and mechanical properties and crystallization behavior of PLA/CNC nanocomposites,” *Carbohydr. Polym.* **123**, 105–114 (2015).
- [42] Arias, A., M.-C. Heuzey, M. A. Huneault, G. Ausias, and A. Bendahou, “Enhanced dispersion of cellulose nanocrystals in melt-processed polylactide-based nanocomposites,” *Cellulose* **22**, 483–498 (2015).
- [43] Safdari, F., P. J. Carreau, M. C. Heuzey, M. R. Kamal, and M. M. Sain, “Enhanced properties of poly(ethylene oxide)/cellulose nanofiber biocomposites,” *Cellulose* **24**, 755–767 (2017).
- [44] Safdari, F., D. Bagheriasl, P. J. Carreau, M. C. Heuzey, and M. R. Kamal, “Rheological, Mechanical, and thermal properties of polylactide/cellulose nanofiber biocomposites,” *Polym. Compos.* **16**, 101–113 (2016).
- [45] Ling, K., H. Jiang, and Q. Zhang, “A colorimetric method for the molecular weight determination of polyethylene glycol using gold nanoparticles,” *Nanoscale Res. Lett.* **8**, 538–548 (2013).
- [46] Pamies, R. R., J. G. Hernández Cifre, M. del Carmen López Martínez and J. García de la Torre, “Determination of intrinsic viscosities of macromolecules and nanoparticles. Comparison of single-point and dilution procedures,” *Colloid Polym. Sci.* **286**, 1223–1231 (2008).
- [47] Brandrup, J., E. H. Immergut, and E. A. Grulke, *Polymer Handbook 4th Edition* (John Wiley, 1999).
- [48] Shulyak, I. V., E. I. Grushova, and a. M. Semenchenko, “Rheological properties of aqueous solutions of polyethylene glycols with various molecular weights,”

- Russ. J. Phys. Chem. A **85**, 419–422 (2011).
- [49] Wu, H., and M. Morbidelli, “Model relating structure of colloidal gels to their elastic properties,” *Langmuir* **17**, 1030–1036 (2001).
- [50] van de Ven, T. G. M., “A model for the adsorption of polyelectrolytes on pulp fibers: relation between fiber structure and polyelectrolyte properties.,” *Nord. Pulp Pap. Res. J.* **15**, 494–501 (2000).
- [51] Khoshkava, V., and M. R. Kamal, “Effect of Surface Energy on Dispersion and Mechanical Properties of Polymer/Nanocrystalline Cellulose Nanocomposites,” *Biomacromolecules* **14**, 3155–3163 (2013).
- [52] Reid, M. S., H. S. Marway, C. Moran-Hidalgo, M. Villalobos, and E. D. Cranston, “Comparison of polyethylene glycol adsorption to nanocellulose versus fumed silica in water,” *Cellulose*, (2017).
- [53] Dang, C. T. Q., Z. J. Chen, N. T. B. Nguyen, W. Bae, and T. H. Phung, “Development of Isotherm Polymer/Surfactant Adsorption Models in Chemical Flooding,” *SPE Asia Pacific Oil Gas Conf. Exhib.*, (2011).
- [54] Sumita, M., K. Sakata, S. Asai, K. Miyasaka, and H. Nakagawa, “Dispersion of fillers and the electrical conductivity of polymer blends filled with carbon black,” *Polym. Bull.* **25**, 265–271 (1991).
- [55] Beuguel, Q., J. Ville, J. Crepin-Leblond, P. Mederic, and T. Aubry, “Influence of clay mineral structure and polyamide polarity on the structural and morphological properties of clay polypropylene/polyamide nanocomposites,” *Appl. Clay Sci.* **135**, 253–259 (2017).
- [56] Wu, S., “Formation of dispersed phase in incompatible polymer blends: Interfacial and rheological effects,” *Polym. Eng. Sci.* **27**, 335–343 (1987).
- [57] Guerrouani, N., A. Mas, and F. Schué, “Synthesis of poly(vinyl alcohol)- graft -poly(ϵ -caprolactone) and poly(vinyl alcohol)- graft -poly(lactide) in melt with magnesium hydride as catalyst,” *J. Appl. Polym. Sci.* **113**, 1188–1197 (2009).
- [58] Van Oss, C. J., *Interfacial Forces in Aqueous Media* (M. Dekker, New York, NY, 1994).
- [59] Edgar, C. D., and D. G. Gray, “Influence of dextran on the phase behavior of suspensions of cellulose nanocrystals,” *Macromolecules* **35**, 7400–7406 (2002).
- [60] S. Wu, *Polymer interface and adhesion* (M. Dekker, 1982).
- [61] Roe, R.-J., “Surface tension of polymer liquids,” *J. Phys. Chem.* **72**, 2013–2017 (1968).
- [62] Carré, A., and K. L. Mittal, *Surface and Interfacial Aspects of Cell Adhesion* (CRC Press, 2011).
- [63] Mobuchon, C., P. J. Carreau, and M.-C. Heuzey, “Effect of flow history on the structure of a non-polar polymer/clay nanocomposite model system,” *Rheol. Acta* **46**, 1045–1056 (2007).
- [64] Dullaert, K., and J. Mewis, “Stress jumps on weakly flocculated dispersions: Steady state and transient results,” *J. Colloid Interface Sci.* **287**, 542–551 (2005).
- [65] Lenfant, G., M.-C. Heuzey, T. G. M. van de Ven, and P. J. Carreau, “A comparative study of ECNC and CNC suspensions: effect of salt on rheological properties,” *Rheol. Acta* **56**, 51–62 (2017).
- [66] Mewis, J., and N. J. Wagner, *Introduction to colloid science and rheology* (Cambridge University Press, Cambridge, 2011).

- [67] Fedors, R. F., “An equation suitable for describing the viscosity of dilute to moderately concentrated polymer solutions,” *Polymer* **20**, 225–228 (1979).
- [68] Lenfant, G., M. C. Heuzey, T. G. M. van de Ven, and P. J. Carreau, “Intrinsic viscosity of suspensions of electrosterically stabilized nanocrystals of cellulose,” *Cellulose* **22**, 1109–1122 (2015).
- [69] Larson, R. G., “The structure and Rheology of Complex Fluids”, (Oxford University, 1999)
- [70] Simha, R., “The Influence of Brownian Movement on the Viscosity of Solutions.,” *J. Phys. Chem.* **44**, 25–34 (1940).
- [71] Galindo-Rosales, F. J., P. Moldenaers, and J. Vermant, “Assessment of the dispersion quality in polymer nanocomposites by rheological methods,” *Macromol. Mater. Eng.* **296**, 331–340 (2011).
- [72] Majesté, J.-C., *Rheology and Processing of Polymer Nanocomposites: Theory, Practice, and New Challenges* (John Wiley & Sons, Inc., Hoboken, NJ, 2016).
- [73] Majesté, J.-C., C. Carrot, B. Olalla, and R. Fulchiron, “Internal reorganization of agglomerates as an explanation of energy dissipation at very low strain for heterogeneous polymer systems,” *Macromol. Theory Simulations* **21**, 113–119 (2012).
- [74] Beuguel, Q., J. Ville, J. Crepin-Leblond, P. Mederic, and T. Aubry, “Comparative study of the structural and rheological properties of PA6 and PA12 based synthetic talc nanocomposites,” *Polymer* **62**, 109–117 (2015).
- [75] Aubry, T., T. Razafinimaro, and P. Médéric, “Rheological investigation of the melt state elastic and yield properties of a polyamide-12 layered silicate nanocomposite,” *J. Rheol.* **49**, 425 (2005).
- [76] Abbasi, S., P. J. Carreau, A. Derdouri, and M. Moan, “Rheological properties and percolation in suspensions of multiwalled carbon nanotubes in polycarbonate,” *Rheol. Acta* **48**, 943–959 (2009).
- [77] Rahatekar, S. S., K. K. Koziol, S. R. Kline, E. K. Hobbie, J. W. Gilman, and A. H. Windle, “Length-dependent mechanics of carbon-nanotube networks,” *Adv. Mater.* **21**, 874–878 (2009).
- [78] Bounoua, S., E. Lemaire, J. Férec, G. Ausias, A. Zubarev, and P. Kuzhir, “Apparent yield stress in rigid fibre suspensions: the role of attractive colloidal interactions,” *J. Fluid Mech.* **802**, 611–633 (2016).
- [79] Shih, W.-H., W. Y. Shih, S.-I. Kim, J. Liu, and I. A. Aksay, “Scaling behavior of the elastic properties of colloidal gels,” *Phys. Rev. A* **42**, 4772–4779 (1990).
- [80] Cherhal, F., F. Cousin, and I. Capron, “Influence of Charge Density and Ionic Strength on the Aggregation Process of Cellulose Nanocrystals in Aqueous Suspension, as Revealed by Small-Angle Neutron Scattering,” *Langmuir* **31**, 5596–5602 (2015).